Weakly bound $p_{3/2}$ neutrons and spin-response function in the many-body pair correlation of neutron drip line nuclei

I. Hamamoto[1,2] and H. Sagawa[3]
[1]*Division of Mathematical Physics, Lund Institute of Technology at the University of Lund, Lund, Sweden*
[2]*The Niels Bohr Institute, Blegdamsvej 17, Copenhagen Ø, DK-2100, Denmark*
[3]*Center for Mathematical Sciences, University of Aizu, Ikki-machi, Aizu-Wakamatsu, Fukushima 965, Japan*
(Received 8 May 2004; published 30 September 2004)

Solving the simplified model of the Hartree-Fock Bogoliubov equation in coordinate space with the correct asymptotic boundary conditions, the spin-orbit splitting, occupation probabilities, effective pair-gap, mean square radius, and spin-response function are studied for weakly bound p neutrons. As the binding energy of $p_{3/2}$ neutrons becomes small or approaches zero, the spin-orbit splitting $p_{3/2}-p_{1/2}$ in the one-body potential drastically decreases and, at the same time, the effective pair-gap for the p neutrons becomes small, while the occupation probability of the $p_{3/2}$ level decreases only slightly. Consequently, in that limit low-lying broader spin response with almost constant amount of total strength appears with the peak moving toward very low excitation energies.

DOI: 10.1103/PhysRevC.70.034317 PACS number(s): 21.60.Ev, 21.10.Pc, 21.60.Jz, 23.20.Lv

I. INTRODUCTION

Weakly bound neutrons with small orbital angular-momentum ℓ play a unique role in neutron drip line nuclei, since they have an appreciable probability to be outside of the core nucleus and are thereby insensitive to the strength of the potential provided by the well-bound nucleons in the system. Those neutrons are especially sensitive to the coupling to the nearby continuum of unbound states and are known to be the origin of halo phenomena, change of shell structure, low-energy threshold strength, unique response functions to various external fields. It was also pointed out in Ref. [1] that extended one-particle wave functions of smaller ℓ orbitals lead to small spin-orbit splitting, due to the smaller probability of those particles around the nuclear surface where the spin-orbit potential is effective.

It is expected that in medium-heavy nuclei the occupancy of low-ℓ weakly bound neutrons will never make a significant contribution to the one-body potential and the many-body pair correlation, partly because the small number of particles which can occupy those orbits and partly because they are weakly coupled to the core nucleus. Neglecting the contribution, we have developed a simplified model of Hartree-Fock Bogoliubov (HFB) [2,3,5].

In Ref. [2,3] the HFB equation in a simplified model was solved in coordinate space with the correct boundary conditions [4–6], and the many-body pair correlation in neutron drip line nuclei was studied for weakly-bound neutrons with various ℓ. Various aspects of weakly bound $s_{1/2}$ neutrons are especially examined in Ref. [3]. We have found that as the one-particle binding energy approaches zero the effective pair gap of $s_{1/2}$ neutrons approaches zero and, thus, the possible $s_{1/2}$ occupation probability in the ground state of even-even nuclei may concentrate on the degree of freedom corresponding to the region of very small quasiparticle energy. Spin response of even-even nuclei may be appropriate for detecting the presence of the low-energy occupation probability. The strength of spin response may be energetically pushed up by possible coupling to other particle-hole (p-h) excitations, but it will not be pushed down, though the coupling is generally expected to be weak for weakly bound low-ℓ neutrons. In order to study response functions for exciting weakly bound low-ℓ neutrons by spin operators, we had better go at least to p neutrons, though very weak excitations of $s_{1/2}$ neutrons by spin operator without radial dependence are obtained in our HFB calculations. We note that the excitation of $s_{1/2}$ neutrons, namely $0\rightarrow 2$ quasiparticle excitations, by the spin operator is forbidden for the pairing field Δ, which does not depend on r. In the present paper we employ the same model as used in Ref. [2,3] and study the spin-response functions of exciting p neutrons and the related phenomena. Comparing the present result with that of Ref. [3], the difference in the basic properties of weakly bound s and p neutrons is exhibited. Our intention is to examine the general properties related to weakly bound low-ℓ neutrons, rather than performing fully self-consistent numerical calculations of HFB for specific nuclei.

In Sec. II we briefly describe our model and related formulas, while numerical results and discussions are given in Sec. III. Conclusions are drawn in Sec. IV.

II. MODEL AND FORMULAS

First, we give a brief summary of our model, which is the same as that used in Ref. [2,3]. We consider the time-reversal invariant and spherically symmetric system with monopole pairing correlation. Considering the coupling of the neutron one-quasiparticle with ℓ and j to the HF field, $V(r)$ and $V_{so}(r)$, and the pairing field $\Delta(r)$, both of which are given by the core nucleus, our HFB equation is reduced to the following coupled equations:

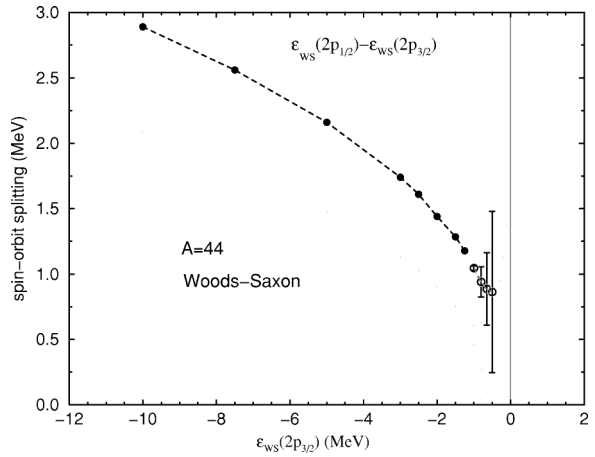

FIG. 1. Spin-orbit splitting, $\varepsilon_{WS}(2p_{1/2})-\varepsilon_{WS}(2p_{3/2})$, calculated in Woods-Saxon potentials, of which the depth is varied so that the $2p_{3/2}$ level is always an eigenstate. The radius of the potential is fixed for $R=r_0A^{1/3}$ with $r_0=1.27$ fm and $A=44$. Filled circles are for the case that the $2p_{1/2}$ level is bound, while open circles express one-particle resonant levels with the width indicated by the length of the vertical line. The one-particle resonant energy is defined so that the calculated phase shift δ passes through $\pi/2$ with positive slope at the one-particle energy, while the width of the resonance is defined by $\Gamma \equiv 2/(d\delta/d\varepsilon)$ estimated at the resonant energy.

$$\left(\frac{d^2}{dr^2}-\frac{\ell(\ell+1)}{r^2}+\frac{2m}{\hbar^2}[\lambda+E_{qp}-V(r)-V_{so}(r)]\right)u_{\ell j} - \frac{2m}{\hbar^2}\Delta(r)v_{\ell j}=0,$$
$$\left(\frac{d^2}{dr^2}-\frac{\ell(\ell+1)}{r^2}+\frac{2m}{\hbar^2}[\lambda-E_{qp}-V(r)-V_{so}(r)]\right)v_{\ell j} + \frac{2m}{\hbar^2}\Delta(r)u_{\ell j}=0, \quad (1)$$

where $u_{\ell j}$ and $v_{\ell j}$ express the upper and lower components of the radial wave functions in the HFB approximation, respectively. We take positive quasiparticle energies $E_{qp}>0$ and consider bound states $\lambda<0$. Then, $(\lambda-E_{qp})$ is always negative, while $(\lambda+E_{qp})$ can be either negative or positive.

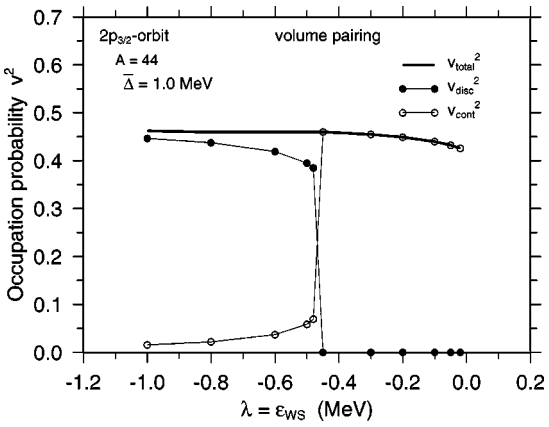

FIG. 2. Occupation probabilities v^2_{disc}, v^2_{cont}, and v^2_{total} for the $2p_{3/2}$ orbit as a function of $\lambda=\varepsilon_{WS}(2p_{3/2})$. Volume-type pairing with $\bar{\Delta}=1$ MeV and the radius of the Woods-Saxon potential $R=r_0A^{1/3}$ with $r_0=1.27$ fm and $A=44$ are used. For $\lambda=\varepsilon_{WS}>-0.46$ MeV there is no discrete solution of the HFB equation (1).

The normalization in the case of $(\lambda+E_{qp})<0$, where E_{qp} is a discrete eigenvalue of the HFB equation, is written as

$$\int_0^\infty (|u_{\ell j}(E_{qp},r)|^2+|v_{\ell j}(E_{qp},r)|^2)dr=1, \quad (2)$$

while in the case of $(\lambda+E_{qp})>0$, where HFB solution exists for any value of E_{qp}, we normalize $u_{\ell j}$ by [2,4,6]

$$\int dr u_{\ell j}(E_{qp},r)u_{\ell j}(E'_{qp},r)=\delta(E_{qp}-E'_{qp}). \quad (3)$$

The normalization of the lower component of the radial wave function $v_{\ell j}$ in the latter case is determined by Eq. (3) via the HFB equation (1), and the quantity

TABLE I. Mean square radii of bound eigenstates of Woods-Saxon potentials, together with the eigenvalues or one-particle resonant energies with widths. The radius for $A=44$ is used for the potential, of which the depth is denoted by V_{WS}. One-particle resonant energies in the continuum and their widths are obtained by the phase shift analysis. See the caption to Fig. 1.

$\varepsilon_{WS}(2p_{3/2})$ (MeV)	V_{WS} (MeV)	$\langle r^2\rangle_{WS}$ $(2p_{3/2})$ (fm^2)	$\varepsilon_{WS}(2p_{1/2})$ (width) (MeV) (keV)	$\langle r^2\rangle_{WS}$ $(2p_{1/2})$ (fm^2)
−10.0	−56.804	17.27	−7.110	18.55
−5.0	−48.225	21.50	−2.841	25.19
−3.0	−44.288	25.45	−1.260	33.58
−2.0	−42.090	29.24	−0.538	46.20
−1.0	−39.593	37.46	0.045(18.4)	
−0.8	−39.032	40.48	0.141(116.0)	
−0.65	−38.59	43.98	0.236(277.0)	
−0.5	−38.124	48.62	0.363(616.0)	
−0.3	−37.45	59.46	$0.644(2.29\times10^3)$	
−0.2	−37.08	70.12	$1.023(1.63\times10^4)$	
−0.1	−36.672	93.94		

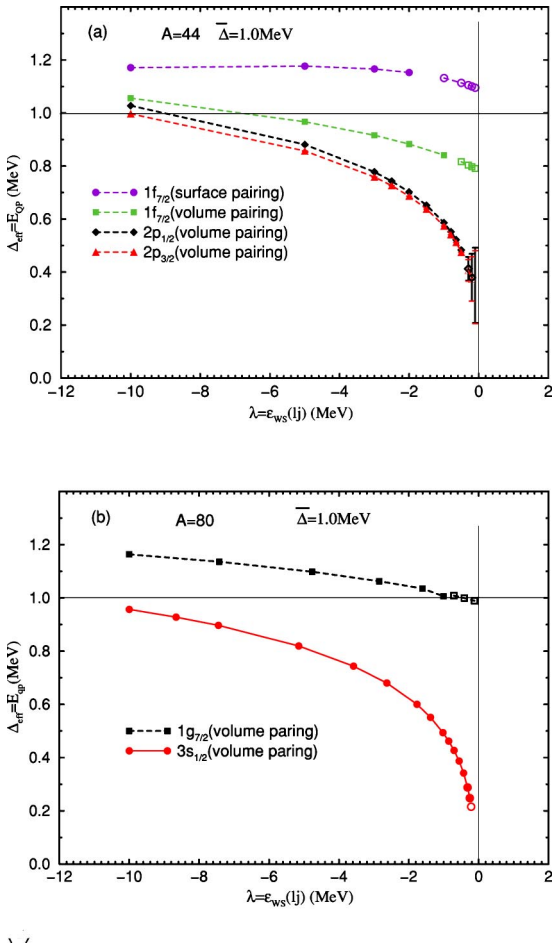

FIG. 3. (Color online) Calculated HFB quasiparticle energies as a function of $\lambda=\varepsilon_{WS}(\ell j)$, where the depth of the Woods-Saxon potentials is varied depending on (ℓj) so that $\varepsilon_{WS}(\ell j)$ is always an eigenvalue of respective potentials. Filled marks express HFB discrete solutions fulfilling the condition $[\lambda+E_{qp}(\ell j)]<0$, while open marks denote the quasiparticle energy at the local maximum of the derivative of the phase shift of $u_{\ell j}$ in the case of $[\lambda+E_{qp}(\ell j)]>0$. The width for the p orbits indicated by the length of vertical lines in (a) is obtained from the energies where the derivative of the phase shift is half of its maximum [6]. In (a) the $1f_{7/2}$, $2p_{3/2}$ and $2p_{1/2}$ orbits are studied with $A=44$, while in (b) the $1g_{7/2}$ and $3s_{1/2}$ orbits are examined with $A=80$.

$$\int_0^\infty |v_{\ell j}(E_{qp},r)|^2 dr \quad \text{where } (\lambda+E_{qp})>0, \tag{4}$$

represents the occupation number probability density per unit energy interval [4].

For simplicity, we replace the HF potential by the Woods-Saxon potential together with the spin-orbit potential, of which the parameters are the standard ones used in β stable nuclei [2,7]. For the given radius $R=r_0A^{1/3}$ with $r_0=1.27$ fm, the diffuseness $a=0.67$ fm and the strength of spin-orbit potential, we vary the potential strength by changing the depth of the Woods-Saxon potential, V_{WS}, so that the corresponding single-particle energy ε_{WS} is varied. Writing

$$f(r)=\frac{1}{1+\exp\left(\dfrac{r-R}{a}\right)}, \tag{5}$$

we have tried the functional form of either the volume-type pairing,

$$\Delta(r)\propto f(r) \tag{6}$$

or the surface-type pairing

$$\Delta(r)\propto r\frac{df(r)}{dr}. \tag{7}$$

The averaged strength of the pair field defined by

$$\bar{\Delta}\equiv\frac{\int_0^\infty r^2 dr\Delta(r)f(r)}{\int_0^\infty r^2 dr f(r)} \tag{8}$$

is an input of numerical calculations expressing the strength of the pair field.

We solve the HFB equation (1) in coordinate space with the correct asymptotic boundary conditions. In numerical integrations we use a radial mesh $\Delta r=0.025$ fm in the neighborhood of the origin $r=0$, while $\Delta r=0.2$ fm is used otherwise. The way of solving the coupled equations (1) is taken from Ref. [8].

It should be emphasized that both the one-body potentials $V(r)$ and $V_{so}(r)$ and the many-body pair field $\Delta(r)$ come almost exclusively from the well bound or weakly bound (but high-ℓ) particles. Thus, in our present work we study the behavior of weakly bound $p_{3/2}$ and/or $p_{1/2}$ neutrons in the many-body pair correlation for given $V(r)$, $V_{so}(r)$, and $\Delta(r)$.

We define the effective pair gap Δ_{eff} by

$$\Delta_{eff}(\ell j)\equiv E_{qp}(\ell j), \tag{9}$$

where the quasiparticle energy $E_{qp}(\ell j)$ is calculated by setting the Fermi level λ satisfying the condition $\lambda=\varepsilon_{WS}(\ell j)$. The effective pair gap defined in this way corresponds to the gap parameter in the BCS approximation, while in the present case of $(\lambda+E_{qp})<0$ it is approximately equal to the smallest quasiparticle energy for a given (ℓj) orbit [2].

We study the response function of the ground state of even-even nuclei, namely the quasiparticle vacuum, to the spin operator $\vec{\sigma}$, using the wave functions $u_{\ell j}$ and $v_{\ell j}$ obtained from solving Eq. (1). In the present study we examine an unperturbed quasiparticle response function, in contrast to the quasiparticle-random-phase approximation (QRPA) response studied in the literature for spin-independent external fields [9,10]. The neglect of RPA correlation may be acceptable, mainly because we are interested in the low-energy threshold strength of drip line nuclei, which is almost decoupled from the well-bound core particles, and partly because the spin-dependent part of the effective interaction (for example, Skyrme interactions) has not been well fixed. Denoting the two quasiparticles by i and j, we have in general

three cases depending on the combination of the signs of $(\lambda+E_i)$ and $(\lambda+E_j)$. For $(\lambda+E_i)<0$ and $(\lambda+E_j)<0$ we obtain the strength

$$B(\omega=E_i+E_j)=|\langle(ij)J^\pi=1^+\|\sigma\|0^+\rangle|^2 = |\langle i\|\sigma\|j\rangle\int_0^{r_{max}} dr[u_i(E_i,r)v_j(E_j,r)-u_j(E_j,r)v_i(E_i,r)]|^2 \tag{10}$$

at a discrete state with $\omega=E_i+E_j$, while in the case of $(\lambda+E_i)<0$ and $(\lambda+E_j)>0$ a continuous spectrum of the strength per unit energy at ω

$$S(\omega=E_i+E_j)=\int dE_j|\langle(ij)J^\pi=1^+\|\sigma\|0^+\rangle|^2\delta(E_i+E_j-\omega) = |\langle i\|\sigma\|j\rangle\int_0^{r_{max}} dr[u_i(E_i,r)v_j(E_j,r)-u_j(E_j,r)v_i(E_i,r)]|^2, \tag{11}$$

where $E_j>|\lambda|$ is a continuous variable, is obtained. When we have both $(\lambda+E_i)>0$ and $(\lambda+E_j)>0$, the response function per unit energy at ω, which is a continuous spectrum starting at $\omega=2|\lambda|$, is calculated by using the formula

$$S(\omega)=\int dE_i\int dE_j|\langle(ij)J^\pi=1^+\|\sigma\|0^+\rangle|^2\delta(E_i+E_j-\omega) = \int_{|\lambda|}^{\omega-|\lambda|} dE_i|\langle i\|\sigma\|j\rangle\int_0^{r_{max}} dr[u_i(E_i,r)v_j(\omega-E_i,r) - u_j(\omega-E_i,r)v_i(E_i,r)]|^2. \tag{12}$$

In the numerical calculations of Eqs. (10)–(12) we use $r_{max}=64$ fm. If for $\omega>2|\lambda|$ both expressions (11) and (12) have nonzero contributions, the sum of Eqs. (11) and (12) is the response of the system. The difference between the dimension of $B(\omega)$ in (10) and that of $S(\omega)$ in Eqs. (11) and (12) comes from the fact that the normalizations of $u_{\ell j}$ and $v_{\ell j}$ are different depending on the sign of $(\lambda+E_{\ell j})$.

The non-energy-weighted sum-rule (NEWSR) and energy-weighted sum-rule (EWSR) are defined as

$$m_0(HFB)=\sum_n B(\omega_n)+\int^{\omega_{max}} d\omega S(\omega) \tag{13}$$

and

$$m_1(HFB)=\sum_n \omega_n B(\omega_n)+\int^{\omega_{max}} \omega d\omega S(\omega), \tag{14}$$

respectively, where $\omega_{max}=10$ MeV is used. In the above Eqs. (13) and (14) the first term on rhs has non-zero contributions only when discrete solutions exist.

We define the occupation probability for $(\lambda+E_{qp})>0$ in the ground state of even-even nuclei by integrating over the relevant energy region

$$v^2_{cont}\equiv\int_{|\lambda|}^{E_{max}} dE_{qp}\int_0^{r_{max}} dr|v_{\ell j}(E_{qp},r)|^2 \tag{15}$$

and that for $(\lambda+E_{qp})<0$ by

$$v^2_{disc}\equiv\int_0^{r_{max}} dr|v_{\ell j}(E^{disc}_{qp},r)|^2, \tag{16}$$

where we use $E_{max}=10$ MeV and $r_{max}=64$ fm. The total occupation probability of the one-particle (ℓj) level is

$$v^2_{total}=v^2_{disc}+v^2_{cont}. \tag{17}$$

The expectation value of mean square radius for $(\lambda+E_{qp})<0$ is defined by

$$\langle r^2\rangle_{disc}\equiv\frac{\int_0^{r_{max}} drr^2|v(E^{disc}_{qp},r)|^2}{v^2_{disc}}, \tag{18}$$

while that for $(\lambda+E_{qp})>0$ by

$$\langle r^2\rangle_{cont}\equiv\frac{\int_{|\lambda|}^{E_{max}} dE\int_0^{r_{max}} drr^2|v(E,r)|^2}{v^2_{cont}}. \tag{19}$$

Thus, the averaged value is written as

$$\langle r^2\rangle_{total}\equiv\frac{\int_0^{r_{max}} drr^2|v(E^{disc}_{qp},r)|^2+\int_{|\lambda|}^{E_{max}} dE\int_0^{r_{max}} drr^2|v(E,r)|^2}{v^2_{disc}+v^2_{cont}}. \tag{20}$$

III. NUMERICAL RESULTS AND DISCUSSIONS

Varying the depth of the Woods-Saxon potential so that the $2p_{3/2}$ state is always an eigenstate, in Fig. 1 we show the calculated spin-orbit splitting, $\varepsilon_{WS}(2p_{1/2})-\varepsilon_{WS}(2p_{3/2})$, as a function of $\varepsilon_{WS}(2p_{3/2})$. Filled circles show the case that the $2p_{1/2}$ level is bound in respective Woods-Saxon potentials, while open circles express that the $2p_{1/2}$ level is a one-particle resonant state with the width indicated by the length

TABLE II. HFB calculations for the volume pairing with $\bar{\Delta}=1$ MeV and $A=44$. The Fermi energy is placed at $\lambda=\varepsilon_{WS}(2p_{3/2})$. Tabulated quantity $v^2(\ell j)$ is $v^2_{total}(\ell j)$ in Eq. (17). The values of E_{qp} and the width in the case of $(\lambda+E_{qp})>0$ are obtained by calculating the derivative of the phase shift. See the text for details.

λ (MeV)	$E_{qp}(2p_{3/2})$ (width) (MeV) (keV)	$v^2(2p_{3/2})$	$\langle r^2\rangle_{total}$ (fm^2)	$E_{qp}(p_{1/2})$ (width) (MeV) (keV)	$v^2(p_{1/2})$	$\langle r^2\rangle_{total}$ (fm^2)
−10.0	0.997	0.481	16.82	3.090	0.025	16.01
−5.0	0.857	0.477	20.49	2.334	0.030	19.17
−3.0	0.759	0.474	23.66	1.891	0.033	21.73
−2.0	0.686	0.471	26.44	1.590	0.035	23.82
−1.0	0.574	0.463	31.71	1.108(74)	0.037	27.48
−0.5	0.475	0.455	37.21	0.861(417)	0.038	30.82
−0.3	0.406(41)	0.455	41.20	0.669(652)	0.038	33.03
−0.2	0.374(84)	0.449	44.11	0.612(801)	0.038	34.55
−0.1	0.343(138)	0.440	48.32	0.586(994)	0.037	36.50

of the vertical line. As the eigenvalue $\varepsilon_{WS}(2p_{3/2})$ increases from −10 MeV to −1 MeV, the spin-orbit splitting is seen to decrease [1] from 3 MeV to 1 MeV.

In Table I the mean square radii calculated for bound eigenstates of Woods-Saxon potentials, together with the eigenvalues and one-particle resonant energies with widths, are shown for the $2p_{3/2}$ and $2p_{1/2}$ orbits.

In Fig. 2 we plot v^2_{disc} from Eq. (16), v^2_{cont} from Eq. (15) and v^2_{total} from Eq. (17) as a function of $\lambda=\varepsilon_{WS}(2p_{3/2})$. The similar figure for the $3s_{1/2}$ orbit can be found in Fig. 8 of Ref. [3]. Using $\bar{\Delta}=1$ MeV, a discrete quasiparticle solution was obtained for $\lambda=\varepsilon_{WS}\leqslant-0.28$ MeV for the $3s_{1/2}$ orbit [3], while it can be obtained for $\lambda=\varepsilon_{WS}\leqslant-0.46$ MeV for the $2p_{3/2}$ orbit. Noting that HFB discrete solutions can be obtained only for $(\lambda+E_{qp})<0$, the minimum value of E_{qp} in the discrete spectra, namely the approximate value of effective pair gap is smaller than 0.28 and 0.46 MeV for the $3s_{1/2}$ and $2p_{3/2}$ orbit, respectively, when the averaged volume-type pair gap $\bar{\Delta}=1$ MeV is used. It is also seen from Fig. 2 that the value of v^2_{total} for the $2p_{3/2}$ orbit decreases very little, as $\lambda=\varepsilon_{WS}(2p_{3/2})$ approaches zero. The range of the value of $\lambda=\varepsilon_{WS}$, in which both v^2_{disc} and v^2_{cont} are appreciable, is narrower for the $2p_{3/2}$ orbit than for the $3s_{1/2}$ orbit.

In Figs. 3(a) and 3(b) we show calculated HFB quasiparticle energies as a function of $\lambda=\varepsilon_{WS}(\ell j)$ using $\bar{\Delta}=1$ MeV, in which the depth of Woods-Saxon potentials is varied depending on the orbit (ℓj) so that $\varepsilon_{WS}(\ell j)$ is always an eigenvalue of respective potentials. In Fig. 3(a) the $1f_{7/2}$, $2p_{3/2}$ and $2p_{1/2}$ orbits are studied and the radius of the potential used is $R=r_0A^{1/3}$ with $r_0=1.27$ fm and $A=44$, while in Fig. 3(b) $A=80$ is used in the study of the $3s_{1/2}$ and $1g_{7/2}$ orbits. In the latter case the radius of the potentials is increased to the one used in [2,3], in order to have the depth of Woods-Saxon potentials to be in a realistic range, say 40–50 MeV. Filled marks express HFB discrete solutions fulfilling the condition $[\lambda+E_{qp}(\ell j)]<0$, while open marks denote the case of $[\lambda+E_{qp}(\ell j)]>0$ in which we plot the quasiparticle energy at the local maximum of the derivative of the phase shift of $u_{\ell j}$. The width of the open marks for the $2p_{3/2}$ and $2p_{1/2}$ orbits indicated by the length of vertical lines in Fig. 3(a) is obtained from the energies where the derivative of the phase shift is half of its maximum [6]. It is seen from Figs. 3(a) and 3(b) that, as $\lambda=\varepsilon_{WS}$ approaches zero, the effective pair gap $\Delta_{eff}(\ell j)$ defined in Eq. (9) approaches zero for the $s_{1/2}$ orbit and becomes very small for the $p_{3/2}$ and $p_{1/2}$ orbits, while it remains comparable to $\bar{\Delta}$ for higher ℓ orbits.

Taking the Fermi level so that the condition $\lambda=\varepsilon_{WS}(2p_{3/2})$ is satisfied, in Table II calculated values of E_{qp}, occupation probabilities v^2_{total}, and mean square radii $\langle r^2\rangle_{total}$ are tabulated. In the case of $(\lambda+E_{qp})>0$ where the calculated width is also shown, the value of E_{qp} is the energy at the local maximum of the derivative of the phase shift of $u_{\ell j}$ and the width is obtained from the energies where the derivative of the phase shift is half of its maximum [6].

In Fig. 4 the mean square radii of the $2p_{3/2}$ and $2p_{1/2}$ orbits calculated by using Woods-Saxon wave functions as a function of ε_{WS} are compared with those in Eq. (20) by HFB wave functions with $\bar{\Delta}=1$ MeV as a function of $\lambda=\varepsilon_{WS}(\ell j)$. When we adjust the depths of respective Woods-Saxon po-

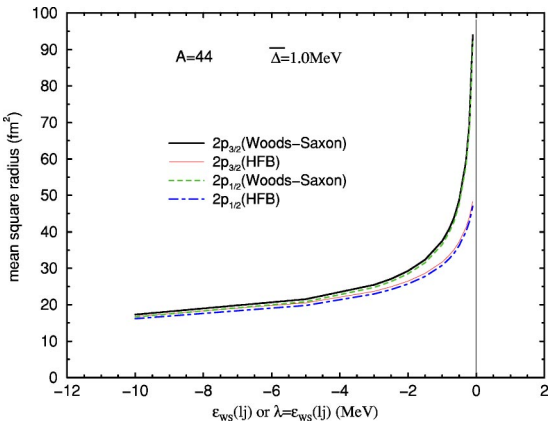

FIG. 4. (Color online) Comparison of the calculated mean square radii of the $2p_{3/2}$ and $2p_{1/2}$ orbits for the Woods-Saxon wave-functions with those of HFB wave functions in Eq. (20). In the former case the x axis denotes the eigenenergy $\varepsilon_{WS}(\ell j)$, while in the latter the x axis expresses $\lambda=\varepsilon_{WS}(2p_{3/2})$ and $\lambda=\varepsilon_{WS}(2p_{1/2})$ for the curves of the $2p_{3/2}$ and $2p_{1/2}$ orbits, respectively.

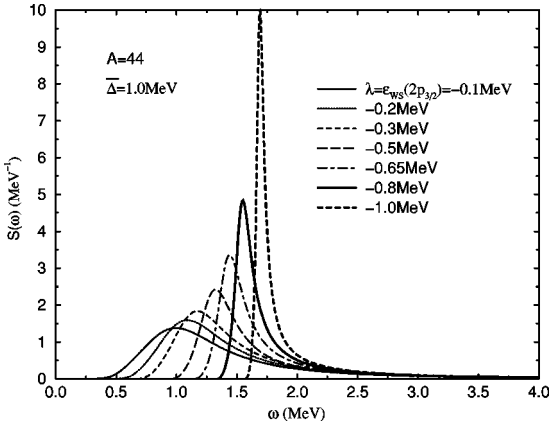

FIG. 5. Spin-response function $S(\omega)$ as a function of excitation energy ω, which is calculated using the HFB wave functions $u_{p_{3/2}}$, $v_{p_{3/2}}$, $u_{p_{1/2}}$, and $v_{p_{1/2}}$ for various values of $\lambda=\varepsilon_{WS}(2p_{3/2})$. The plotted quantity is the sum of $S(\omega)$ in Eqs. (11) and (12). See the text for details.

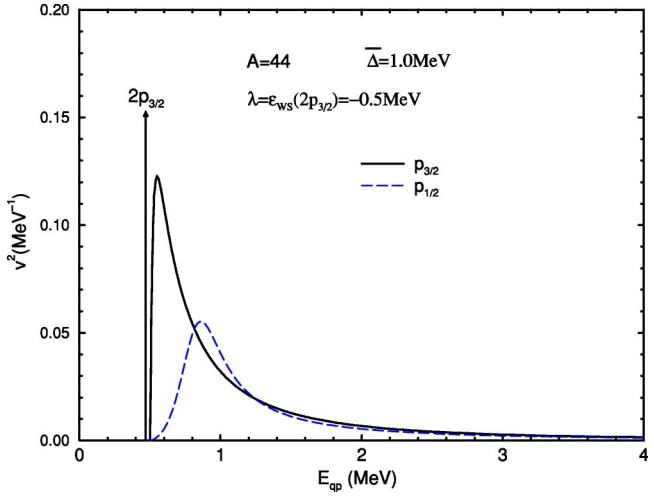

FIG. 6. (Color online) Occupation probability (4) calculated from HFB solutions for both the $p_{3/2}$ and $p_{1/2}$ orbits in the case of $\lambda=\varepsilon_{WS}(2p_{3/2})=-0.5$ MeV. The quasiparticle energy of the HFB discrete solution, $E_{qp}^{disc}(2p_{3/2})=0.475$ MeV, is denoted by the vertical arrow.

tentials so that $\varepsilon_{WS}(2p_{3/2})=\varepsilon_{WS}(2p_{1/2})$ or for the same values of $\lambda=\varepsilon_{WS}(2p_{3/2})$ and $\lambda=\varepsilon_{WS}(2p_{1/2})$, the calculated mean square radius of the $2p_{3/2}$ orbit is slightly larger than that of the $2p_{1/2}$ orbit, due to different signs of the spin-orbit potentials. As $\lambda=\varepsilon_{WS}$ approaches zero, the mean square radius for p orbits in HFB increases appreciably, while the one in the Woods-Saxon potential approaches infinity as ε_{WS} goes to zero.

In Fig. 5 we show the spin response $S(\omega)$ as a function of excitation energy ω, which is calculated using the HFB wave functions $u_{p3/2}$, $v_{p3/2}$, $u_{p1/2}$, and $v_{p1/2}$ for various values of $\lambda=\varepsilon_{WS}(2p_{3/2})$. The plotted quantity is the sum of $S(\omega)$ from Eqs. (11) and (12). There is no contribution by $B(\omega)$ from Eq. (10) in the plotted range of the variable $\varepsilon_{WS}(2p_{3/2})$, since no HFB discrete solution for the $2p_{1/2}$ orbit is obtained for the Woods-Saxon potential which gives $\varepsilon_{WS}(2p_{3/2})\geqslant -1.0$ MeV. For the parameter values $\lambda=\varepsilon_{WS}(2p_{3/2})<-0.46$ MeV the strength $S(\omega)$ appears at much lower values than $\omega=2|\lambda|$, due to the contribution by $S(\omega)$ in (11), namely due to the presence of the HFB discrete solution for the $2p_{3/2}$ orbit where $E_{qp}^{disc}(2p_{3/2})<|\lambda|$. For reference, the occupation probability (4) of HFB solutions for both the $2p_{3/2}$ and $2p_{1/2}$ orbits is shown for $\lambda=\varepsilon_{WS}(2p_{3/2})=-0.5$ MeV in Fig. 6, where the $2p_{3/2}$ quasiparticle energy of the HFB discrete solution, $E_{qp}^{disc}=0.475$ MeV, is denoted by the vertical arrow. It is seen from Fig. 5 that as the value of $\lambda=\varepsilon_{WS}(2p_{3/2})$ increases from -1.0 MeV and approaches zero, the spin response function becomes broader and, at the same time, the major strength shifts to the region of smaller ω values, which are indeed much smaller than $2\bar{\Delta}=2$ MeV.

Though it may be estimated from Fig. 5 that the NEWSR remains nearly unchanged as $\lambda=\varepsilon_{WS}(2p_{3/2})$ increases from

TABLE III. Spin Response Sum Rules in $A=44$. $\omega_{max}=10$ MeV, $\lambda=\varepsilon_{WS}(2p_{3/2})$ and volume pairing with $\bar{\Delta}=1$ MeV are used. E_x (HFB) is the sum of the two discrete quasiparticle energies for $\lambda<-1$ MeV, while it is the peak energy of the response in the case that the response becomes continuous, namely for $\lambda\geqslant -1$ MeV. See the text for details.

$\varepsilon_{WS}(2p_{3/2})=\lambda$ (MeV)	E_x (BCS) (MeV)	m_0 (BCS)	m_1 (BCS) (MeV)	E_x (HFB) (MeV)	m_0 (HFB)	m_1 (HFB) (MeV)
−10.0	4.06	1.794	7.28	4.09	1.735	7.09
−5.0	3.38	1.546	5.23	3.19	1.623	5.18
−3.0	3.01	1.338	4.03	2.65	1.584	4.40
−2.0	2.75	1.146	3.15	2.28	1.543	3.82
−1.0	2.45	0.823	2.02	1.69	1.527	3.22
−0.8	2.37	0.724	1.72	1.55	1.510	3.04
−0.65	2.34	0.671	1.57	1.44	1.497	2.89
−0.5				1.35	1.484	2.74
−0.3				1.17	1.479	2.53
−0.2				1.09	1.450	2.37
−0.1				1.00	1.418	2.18

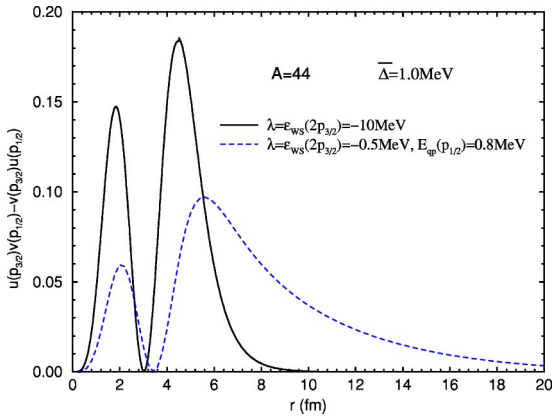

FIG. 7. (Color online) Examples of the dependence of the HFB pairing factor $(u_{2p_{3/2}}v_{p_{1/2}}-v_{2p_{3/2}}u_{p_{1/2}})$ on radial variable. For $\lambda=\varepsilon_{WS}(2p_{3/2})=-10$ MeV all radial wave functions, $u_{2p_{3/2}}$, $v_{2p_{3/2}}$, $u_{p_{1/2}}$, and $v_{p_{1/2}}$ are bound-state wave functions. For $\lambda=\varepsilon_{WS}(2p_{3/2})=-0.5$ MeV together with $E_{qp}(p_{1/2})=0.8$ MeV, both $v_{2p_{3/2}}$ and $v_{p_{1/2}}$ are bound-state wave functions, however, $u_{p_{1/2}}$ is a continuum wave function while $u_{2p_{3/2}}$ can be either a bound or continuum (for $E_{qp}>|\lambda|=0.5$ MeV) wave function. (See, for example, Fig. 6: the occupation probability $v^2_{2p_{3/2}}$ becomes continuous in E_{qp} for continuum wave functions $u_{2p_{3/2}}$.) In the figure the bound-state wave function $u_{2p_{3/2}}$ $(E^{disc}_{qp}(2p_{3/2})=0.475$ MeV$,r)$ is used. A comparison between two curves in the figure should be made only in their radial shape, since the dimension of $(u_{2p_{3/2}}v_{p_{1/2}}-v_{2p_{3/2}}u_{p_{1/2}})$ is different in two examples.

-1.0 MeV to -0.1 MeV, in Table III we list the calculated HFB sum rules together with either the sum of the two quasiparticle energies in the case of the discrete response or the peak energy in the case of the continuous response. In order to clarify the effect of the presence of nearby continuum taken into account in the HFB calculation, our HFB result is compared with the simplest version of BCS calculations. The latter is estimated using the usual BCS formulas with the pair-gap $\Delta=1$ MeV and one-particle eigenenergy (or resonant energy) $\varepsilon_{WS}(\ell j)$ that is calculated for the Woods-Saxon potentials used for respective HFB calculations. The overlap between the $2p_{3/2}$ and $2p_{1/2}$ wave functions is taken to be unity as in the harmonic-oscillator model. The NEWSR of the BCS estimate, m_0(BCS), decreases strongly as $\lambda=\varepsilon_{WS}(2p_{3/2})$ increases, due to the strongly decreasing spin-orbit splitting, $\varepsilon_{WS}(2p_{1/2})-\varepsilon_{WS}(2p_{3/2})$, which makes the relevant BCS pairing factor $|U_{2p_{3/2}}V_{2p_{1/2}}-V_{2p_{3/2}}U_{2p_{1/2}}|$ much smaller. Note that in the limit of small spin-orbit splitting compared with pair gap the BCS pairing factor $|U_{2p_{3/2}}V_{2p_{1/2}}-V_{2p_{3/2}}U_{2p_{1/2}}|$ approaches zero. Here we denote the BCS occupation and unoccupation amplitudes by $U_{\ell j}$ and $V_{\ell j}$, respectively, which are just numbers and do not depend on r. In contrast, the NEWSR from the HFB calculation, m_0(HFB), remains almost unchanged when $\lambda=\varepsilon_{WS}(2p_{3/2})$ increases approaching zero, because the effective pair-gap Δ_{eff} for the p orbits in the HFB calculation decreases at the same time as the spin-orbit splitting becomes small. This feature of the HFB result does not depend on the position of the Fermi level used in the calculation.

Since our system is a bound system, the lower components of the HFB radial wave functions $v_{\ell j}$ are bound-state wave functions, however, the upper components $u_{\ell j}$ are continuum wave functions in the case of $(\lambda+E_{qp})>0$. The orthogonality (3) of those continuum $u_{\ell j}(E_{qp},r)$ functions, for example, can be numerically obtained, only when the radial integral is carried out to infinity. To perform such a numerical integration is practically impossible. Therefore, it is not easy to make a reliable numerical estimate of response to one-particle operators, which contain a factor $u_{\ell j}u_{\ell' j'}$ in the case that none of $u_{\ell j}$ and $u_{\ell' j'}$ are bound-state wave functions. The spin response, which we study in the present work, contains the pairing factor $(u_{2p_{3/2}}v_{p_{1/2}}-v_{2p_{3/2}}u_{p_{1/2}})$, where $v_{\ell j}(E_{qp},r)$ are always bound-state wave functions. Therefore, the spin response can be reliably estimated. In Fig. 7 we show examples of the radial dependence of the HFB pairing factor $(u_{2p_{3/2}}v_{p_{1/2}}-v_{2p_{3/2}}u_{p_{1/2}})$, in order to demonstrate the reliability of the present numerical results. As seen in Fig. 7, when $\lambda=\varepsilon_{WS}(2p_{3/2})$ approaches zero, the HFB pairing factor starts to have a long tail in radial coordinate. We have checked that the numerical values of $S(\omega)$, m_0(HFB) and m_1(HFB) estimated with $r_{max}=64$ fm in Eqs. (11) and (12), which are given in the present paper, are reliable, thanks to the fact that our spin operator has no radial dependence.

IV. CONCLUSIONS

We have studied the properties of weakly bound p neutrons and the related spin response functions, solving a simplified model of the HFB equation in coordinate space with the correct asymptotic boundary conditions. When the binding energy of $p_{3/2}$ neutrons in the Woods-Saxon potential approaches zero, we have shown: (a) the spin-orbit splitting $p_{1/2}-p_{3/2}$ in the one-particle energy spectra decreases drastically; (b) the total occupation probability of the $p_{3/2}$ level decreases only slightly; (c) the effective pair gap for the p neutrons becomes very small; (d) the mean square radius becomes appreciably large; (e) an appreciable amount of spin response appears at excitation energies much lower than $2\bar{\Delta}$; (f) the NEWSR of spin response in the HFB result decreases only slightly compared with that of BCS calculations.

ACKNOWLEDGMENT

This work was supported in part by the Japanese Ministry of Education, Science, Sports and Culture by Grant-In-Aid for Scientific Research under Program No. C(2) 16540259.

[1] I. Hamamoto, S. Lukyanov, and X. Z. Zhang, Nucl. Phys. **A683**, 255 (2001).
[2] I. Hamamoto and B. R. Mottelson, Phys. Rev. C **68**, 034312 (2003).
[3] I. Hamamoto and B. R. Mottelson, Phys. Rev. C **69**, 064302 (2004).
[4] A. Bulgac, Institute of Atomic Physics Preprint No. FT-194-1980, 1980, nucl-th/9907088.
[5] S. T. Belyaev, A. V. Smirnov, S. V. Tolokonnikov, and S. A. Fayans, Yad. Fiz. **45**, 1263 (1987) [Sov. J. Nucl. Phys. **45**, 783 (1987)].
[6] M. Grasso, N. Sandulescu, Nguyen Van Giai, and R. J. Liotta, Phys. Rev. C **64**, 064321 (2001).
[7] A. Bohr and B. R. Mottelson, *Nuclear Structure* (Benjamin, Reading, MA, 1969), Vol. I.
[8] T. Tamura, Oak Ridge National Laboratory Report No. ORNL-4152, UC-32—Mathematics and Computers, 1967.
[9] M. Matsuo, Nucl. Phys. **A696**, 371 (2001).
[10] E. Khan, N. Sandulescu, M. Grasso, and N. Van Giai, Phys. Rev. C **66**, 024309 (2002).